JACS
JOURNAL OF THE AMERICAN CHEMICAL SOCIETY
Article
pubs.acs.org/JACS

Closely Stacked Oligo(phenylene ethynylene)s: Effect of π-Stacking on the Electronic Properties of Conjugated Chromophores

Subodh P. Jagtap, Sukrit Mukhopadhyay, Veaceslav Coropceanu, Glen L. Brizius, Jean-Luc Brédas, and David M. Collard*

School of Chemistry and Biochemistry and Center for Organic Photonics and Electronics, Georgia Institute of Technology Atlanta, Georgia 30332-0400, United States

Supporting Information

ABSTRACT: In this work, a bicyclo[4.4.1]undecane scaffold is used to hold oligo(phenylene ethynylene) units in a cofacially stacked arrangement along the entire length of the conjugated units. We study the impact that the resulting strong interchain interactions have on the photophysical properties. The length of the individual oligomer branches was varied from three to five rings to investigate the effect of conjugation on the electronic properties of the stacked segments. Absorption and fluorescence spectra were recorded and compared to those of the corresponding unstacked analogues. Time-dependent density functional theory calculations were carried out and helped to rationalize the low-energy features present in the fluorescence spectra of the stacked systems. The calculations indicate that the low-energy emissions are due to the presence of excimer-like states. The stronger intensity of the low-energy fluorescence band observed in the five-ring stacked system compared to the three-ring analogue is attributed to the smaller activation barrier that separates the local intrachain state and the excimer-like state in the former compound.

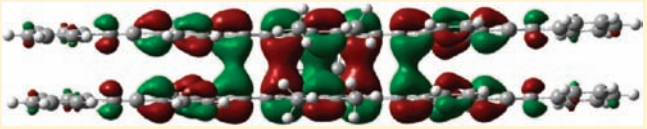

INTRODUCTION

It is well established that π-conjugated organic molecules and polymers present a strong relationship between their geometric and electronic structures.[1−6] This relationship manifests clearly when it comes to a description of the optoelectronic properties,[7] since an electronic excitation can lead to significant modifications of the intra- and intermolecular geometries[8,9] that in turn modify the electronic structure. Thus, the design of new materials with optimal properties for organic electronics applications such as organic field-effect transistors,[10−12] light-emitting diodes,[13−15] or solar cells[16−18] requires a fundamental understanding of this relationship. In this respect, model compounds with well-defined geometries containing only a few interacting conjugated segments prove to be very useful, since they allow for a comprehensive study that combines spectroscopic techniques with high-level theoretical methods.

Various scaffolds have been used in order to hold pairs of conjugated units atop one another. These include, for instance, [2,2]paracyclophane,[19−22] calix[4]arene,[23] arene-annelated bicyclo[4.4.1]undecane,[24−27] 4,5-disubstituted xanthene,[28,29] *m*-terphenyl oxacyclophane,[30] and macrocyclic oligothiophenes.[31] Stacked assemblies of conjugated systems appended to these scaffolds allow for the detailed exploration of the effect of π−π interactions on the optoelectronic properties of π-conjugated chains. For example, Bazan and co-workers have explored the through-space interactions between pairs of stilbenes[32] or phenylene ethynylenes[19] by using a pseudopara disubstituted [2.2]paracyclophane scaffold to hold the chromophores in a stacked arrangement, e.g., **CP**[**PE**$_3$]$_2$ in Figure 1.[19] Such stacked compounds display considerably larger Stokes shifts than the analogous linear unstacked chromophores. This is ascribed to absorption by a single chromophoric moiety, followed by relaxation to a lower energy "phane" state that results from through-space interactions between the stacked π-systems within the cyclophane core. However, in these instances only the terminal phenyl rings of each conjugated moieties are held in a stacked arrangement (i.e., those of the cyclophane core). This situation is in contrast to the close-packed interaction along the entire length of conjugated oligomers or between extended segments of conjugated polymers, as is the case in thin films of many organic semiconductors.[33]

In a recent study of the effect of stacking of conjugated oligomers on the formation of cationic species as models for bipolaron-like charge carriers, we used the bicyclo[4.4.1]-undecane scaffold to hold pairs of terthiophene or pentathiophene units in a stacked arrangement, e.g., *st*-[**Th**$_3$]$_2$ in Figure 1.[26] Here, we append linear oligo(phenylene ethynylene) units to this scaffold to form compounds with a well-defined π-stacked arrangement and use these to explore the effect of stacking on the photophysical properties of conjugated systems. The use of this scaffold results in the possibility of strong interactions along the entire length of the conjugated segments. As an initial step toward a better understanding of the properties of the stacked compounds and of the impact of such extended interchain interactions on the photophysics, we describe here simple absorption and fluorescence measurements complemented by detailed quantum-mechanical calculations.

Received: February 27, 2012
Published: March 28, 2012

   dx.doi.org/10.1021/ja3019065 | *J. Am. Chem. Soc.* 2012, 134, 7176−7185

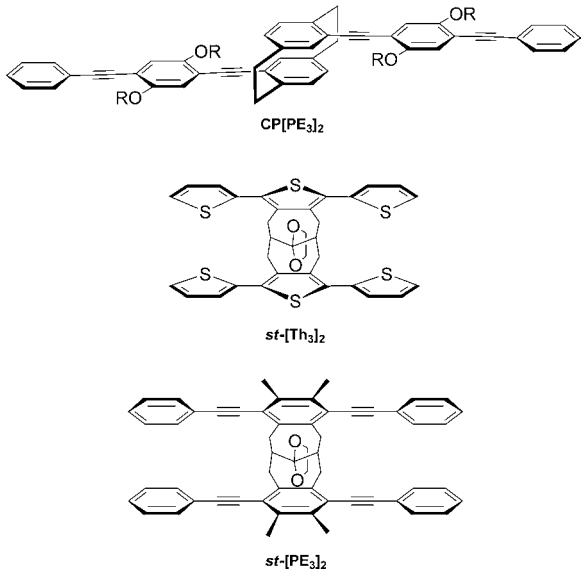

Figure 1. Stacked conjugated compounds: Pseudopara [2.2]-paracyclophane stacked oligo(phenylene ethynylene) **CP**[$\mathbf{PE_3}$]$_2$ (R = n-$C_{12}H_{25}$), in which only the terminal phenylene unit of the conjugated oligomers are held in a stacked arrangement (ref 7); dithieno-fused bicyclo[4.4.1]undecane stacked terthiophene, ***st***-[$\mathbf{Th_3}$]$_2$ (ref 10); and benzo-annelated bicyclo[4.4.1]undecane based stacked oligo(phenylene ethynylene), ***st***-[$\mathbf{PE_3}$]$_2$.

RESULTS AND DISCUSSION

Synthesis of Stacked and Unstacked Model Compounds. Tetramethyl-substituted benzo-annelated bicyclo[4.4.1]undecanone **1** was prepared by treating dimethyl 1,3-acetonedicarboxylate with 1,2-bis(bromomethyl)-4,5-dimethylbenzene followed by saponification and decarboxylation according to the methods described by Mataka, Figure 2.[24] We incorporated the four methyl groups on the fused arenes so as to direct the subsequent placement of the conjugated arms to the ortho positions and thereby provide the linear conjugated oligomeric segments. Ketone **1** was iodinated (I_2, $Hg(OTf)_2$) to provide the tetraiodo compound **2**. Sonogashira cross-coupling of **2** and phenylene ethynylene arms (see the Supporting Information) followed by ketalization afforded the stacked analogs ***st***-[$\mathbf{PE_3}$]$_2$ and ***st***-[$\mathbf{PE_5}$]$_2$; ketalization of **1** affords **3** (***st***-[$\mathbf{PE_1}$]$_2$). Ketalization forces the two seven-membered rings of the bicyclo[4.4.1]undecane scaffold into a pseudo chair/pseudo chair conformation, thus stacking the fused oligomers atop one another. Unstacked analogues of the covalently stacked conjugated oligomers were prepared by analogous Sonogashira coupling of phenylene ethynylene arms to commercially available 2,3,5,6-tetramethyl-1,4-diiodobenzene.

NMR Spectral Analysis. The ^{1}H NMR spectrum of **3** (***st***-[$\mathbf{PE_1}$]$_2$) confirms that the seven-membered rings of the bicyclo[4.4.1]undecane core are in a pseudo chair conformation such that the fused benzene rings are stacked atop one another. The diastereotopic hydrogen atoms of the benzylic methylene groups of ***st***-[$\mathbf{PE_1}$]$_2$ give rise to a pair of doublets of doublets at δ 3.34 (J_{gem} = 15 Hz, J_{vic} = 2 Hz) and δ 2.58 (J_{gem} = 15, J_{vic} = 6 Hz) for the equatorial and axial positions, respectively. The stacked nature of the arenes causes an upfield shift of the singlet for the aromatic hydrogen atoms of **3** (δ 6.39) relative the corresponding singlet of the unstacked linear analog **1** (δ 6.85). Accordingly, the methyl groups on the bicycloundecane core do not interfere with the stacking noted by Mataka for the unsubstituted benzo-fused bicycle.[24]

The phenylene ethynylene arms of ***st***-[$\mathbf{PE_3}$]$_2$ and ***st***-[$\mathbf{PE_5}$]$_2$ do not impede the adoption of a stacked conformation by the bicyclic scaffold. The ^{1}H NMR spectrum of ketone [$\mathbf{PE_3}$]$_2$ exhibits a series of broad peaks at 2.8−3.5 ppm due to the time-averaged signal of the benzylic protons in the rapidly interconverting pseudo chair/chair, chair/boat, and boat/boat conformations of the bicyclic core. Ketalization of ketone [$\mathbf{PE_3}$]$_2$ provides the stacked trimer ***st***-[$\mathbf{PE_3}$]$_2$, which exhibits of a pair of doublets of doublets at δ 3.79 (J = 15, 6 Hz) and δ 3.30 (J = 15, 2 Hz) for the diastereotopic benzylic hydrogen atoms. As with the single ring analog **3**, there is an upfield shift in the signals corresponding to the aromatic protons from δ 7.20−7.70 for the linear analog $\mathbf{PE_3}$ to δ 7.10−7.40 for the stacked ketal ***st***-[$\mathbf{PE_3}$]$_2$. A similar set of peaks is observed for the benzylic and aromatic protons of the analogous stacked

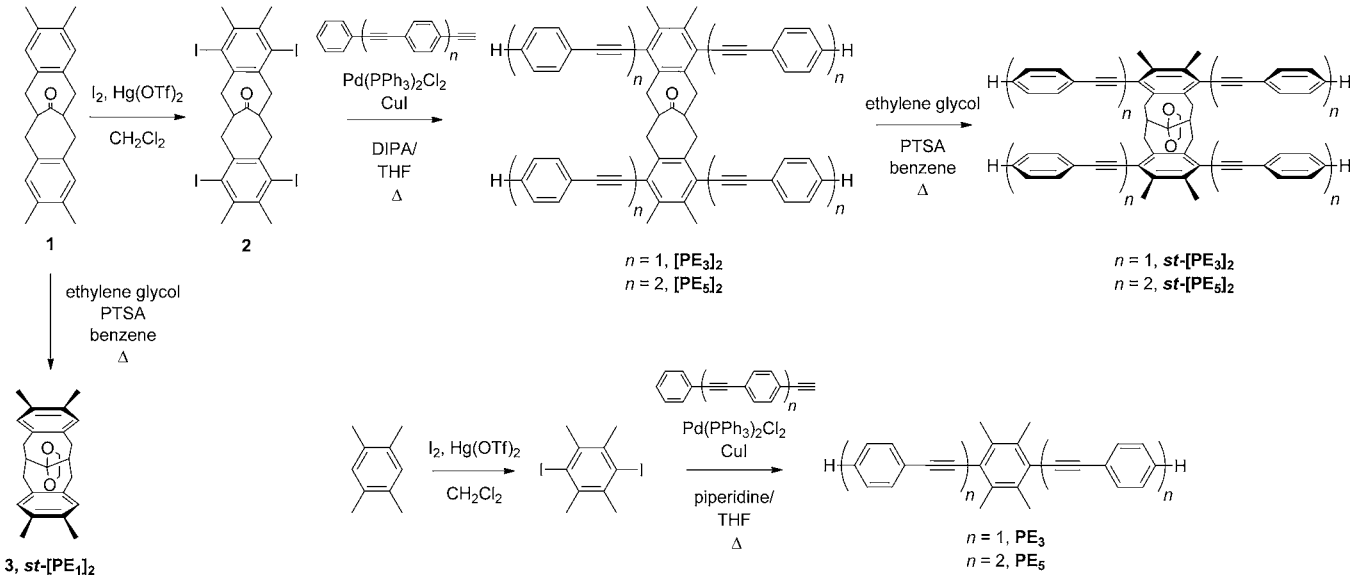

Figure 2. Synthesis of stacked compounds **3** (***st***-[$\mathbf{PE_1}$]$_2$), ***st***-[$\mathbf{PE_3}$]$_2$, and ***st***-[$\mathbf{PE_5}$]$_2$ and of the simple linear analogs $\mathbf{PE_3}$ and $\mathbf{PE_5}$.

dx.doi.org/10.1021/ja3019065 | J. Am. Chem. Soc. 2012, 134, 7176−7185

pentamer, *st*-$[PE_5]_2$: The benzylic hydrogen atoms give rise to a doublets of doublets at δ 3.84 (J = 15, 6 Hz) and δ 3.30 (J = 15, 2 Hz), and the multiplet for the hydrogen atoms on the phenylene ethynylene arms is shifted slightly upfield compared to the unstacked analog, PE_5 (see the Supporting Information), suggesting that it also adopts a stacked architecture in solution.

X-ray Crystal Structures. The X-ray crystal structure of ketal *st*-$[PE_1]_2$ confirms that the bicycloundecanone core adopts a pseudo chair/chair conformation with a cofacially stacked arrangement of the fused benzene rings. The distance between the centers of the stacked benzene rings (d_1) is 3.42 Å, Figure 3 (top) and Table 1. The benzene rings are tilted at an angle (θ_1) of 16.8° with respect to one another: The inner pairs of aromatic carbon atoms (i.e., those fused to the bicyclic structure) are 3.03 Å apart, whereas the outer pairs (i.e., those bearing methyl substituents) are held at a distance of 3.74 Å. Thus, this conformation is similar to that reported by Mataka for the compound lacking the methyl substituents (d_1 = 3.56 Å; θ_1 = 25°).

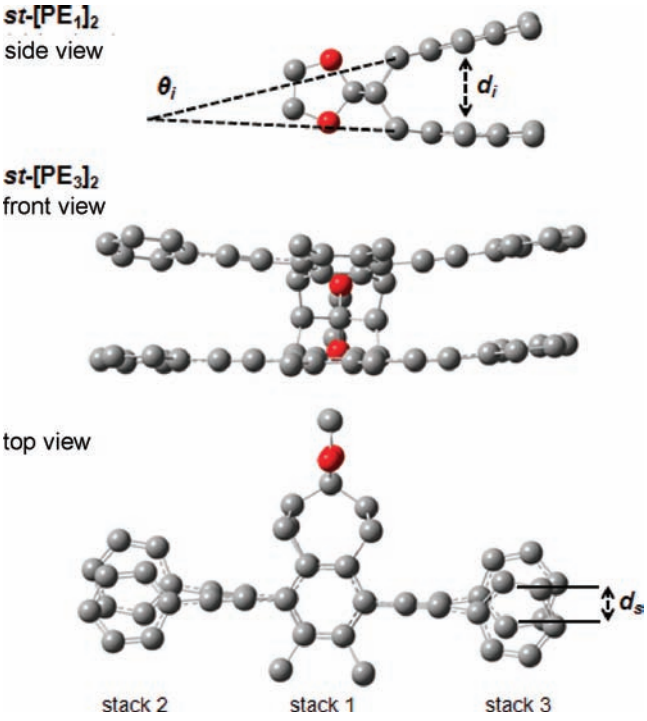

Figure 3. X-ray crystal structure of *st*-$[PE_1]_2$ (side view), and *st*-$[PE_3]_2$ (front and top views); d_i represents the intercentroid distance, θ_i the interplane angle between the stacked phenyl rings, and d_s the slip distance between the stacked rings.

Similarly, the X-ray crystal structure of *st*-$[PE_3]_2$ confirms a pseudo chair/chair conformation for the bicyclic scaffold in the presence of the phenylene ethynylene arms, Figure 3 (middle and bottom). The central rings of the stacked conjugated trimer moieties are separated by an intercentroid distance (d_1) of 3.42 Å, with a tilt angle (θ_1) of 17.9° between them. The dihedral angles between the bridgehead and benzylic hydrogens inferred from the crystallographic data are consistent with the coupling constants obtained from ^{1}H NMR analysis of solutions of the ketals: The 6 Hz coupling constant between the bridgehead and equatorial benzylic hydrogen atom is consistent with dihedral angle of 52° using the Karplus equation,[34] and the 47° dihedral angle between the bridgehead and axial position results in a 2 Hz coupling. Thus, comparison of the conformation of the cores of *st*-$[PE_1]_2$ and *st*-$[PE_3]_2$ indicates that the incorporation of the four arms does not cause repulsion between the conjugated moieties, and that the stacked chair/chair conformation observed in the solid state is preserved in solution.

The X-ray crystal structure of *st*-$[PE_3]_2$ also indicates that the peripheral rings are in a stacked arrangement, although there occur slight distortions from planarity and linearity in the stacked trimeric segments. The intercentroid distances between pairs of rings on the periphery of the molecule are 3.84 Å (d_2) and 4.01 Å (d_3), Figure 3 (middle). The larger intercentroid distance between these pairs (referred to hereafter as "stack 2" and "stack 3") compared to the central pair ("stack 1", separated by d_1) results from a small in-plane bending of one conjugated segment toward, and the other away from, the bicyclic scaffold, Figure 3 (bottom). This results in an offset between the pairs of peripheral rings that we characterize by a slip distance (d_s), Figure 3 (bottom). The peripheral rings in *st*-$[PE_3]_2$ are tilted out of the plane of the central aromatic rings by an average of only 5°, thereby retaining conjugation along the entire length of each segment in the stacked arrangement. Being unconstrained by fusion to the scaffold itself, the pairs of peripheral rings adopt a more coplanar arrangement (θ_2 = 1.7°;

Table 1. Comparison of Selected Structural Parameters (Distances, d_i, and Angles, θ_i) of the Stacked Compounds *st*-$[PE_x]_2$ (x = 1, 3, 5) from X-ray Diffraction and DFT Optimization of Ground-State (gs) and Excited-State (ex) Geometries

	intercentroid distance, d_i (Å)					interplane angle, θ_i (°)				
geometry	d_1	d_2	d_3	d_4	d_5	θ_1	θ_2	θ_3	θ_4	θ_5
					X-ray Crystallography					
st-$[PE_1]_2$	3.42					16.8				
st-$[PE_3]_2$	3.42	3.81	4.00			17.9	1.7	11.9		
					ωB97X-D/6-31g*					
st-$[PE_3]_2$										
gs	3.39	3.76	3.76			15.5	1.4	1.5		
gs ($CHCl_3$)	3.39	3.78	3.78			12.8	1.6	1.7		
ex	3.15	3.54	3.54			10.8	4.9	4.6		
st-$[PE_5]_2$										
gs	3.39	3.69	3.69	3.79	3.80	13.6	0.6	1.4	2.0	2.2
gs ($CHCl_3$)	3.40	3.68	3.68	3.82	3.81	12.8	0.7	1.6	1.2	1.8
ex	3.17	3.47	3.47	3.71	3.71	11.0	0.2	1.4	1.3	1.8

dx.doi.org/10.1021/ja3019065 | J. Am. Chem. Soc. 2012, 134, 7176–7185

θ_3 = 11.9°) than the central rings (θ_1 = 17.9°). We ascribe the small differences in the torsion angle between the pairs of phenylene ethynylenes on each side of the scaffold to crystal packing forces since these differences are absent in our DFT-optimized geometries. We note that the optimized geometries lead to θ_1 and θ_2 values between 1°−2°. The stacked pentamer, ***st***-$[\mathbf{PE}_5]_2$, does not provide diffraction-quality crystals to allow a similar crystallographic analysis.

DFT-Optimized Ground-State Geometries. The optimized geometries of the ground state of ***st***-$[\mathbf{PE}_3]_2$ and of ***st***-$[\mathbf{PE}_5]_2$ were obtained using the ωB97XD functional with the 6-31 g* basis set. We considered both the isolated molecules and the molecules embedded in a dielectric continuum taking implicit account of the solvent (here, $CHCl_3$ that corresponds to ε = 4.7). The calculations reveal that the solvent has only a marginal effect on the optimized ground-state geometry in both systems (Table 1). The DFT-derived geometry of ***st***-$[\mathbf{PE}_3]_2$ compares well with that obtained from the crystal structure, Table 1. In particular, the calculations reproduce well the slight nonlinearity and twisting of the two conjugated tiers. The slip displacement of the peripheral benzene rings apparent in the top view of the calculated geometry (Figure 4, top) closely matches that observed in the X-ray crystal structure, Figure 3 (bottom). In the optimized geometry of the ground state, the slip distance within both of the peripheral stacks (2 and 3) is 1.65 Å; in the X-ray crystal structure, the slip distance between the benzene rings in stack 2 and stack 3 of ***st***-$[\mathbf{PE}_3]_2$ is ca. 1.55 Å.

For the stacked pentamer ***st***-$[\mathbf{PE}_5]_2$, the intercentroid distances, torsional angles, and slip distances between the inner pairs of stacked rings (stacks 2 and 3, d_s = 1.60 Å) are comparable to those in the stacked trimer, ***st***-$[\mathbf{PE}_3]_2$. The slip distances between the pairs of external rings of ***st***-$[\mathbf{PE}_5]_2$ (stacks 4 and 5) are only slightly larger (1.70 Å) than for the inner pairs. Thus, this result reinforces the contention that the conjugated pentamer units are held in close proximity over their entire length.

UV−Visible and Fluorescence Spectroscopies. The stacked oligomers and unstacked linear analogues were characterized by UV−vis and fluorescence spectroscopies to explore the effect of stacking on the electronic structure of the conjugated moieties. The absorption maximum of the stacked trimer, ***st***-$[\mathbf{PE}_3]_2$, (330 nm) is blue-shifted by 60 meV relative to that of the unstacked linear analog $\mathbf{PE}_3$ (325 nm). As seen from Figure 5, the absorption edge of ***st***-$[\mathbf{PE}_3]_2$ contains a low-energy tail, which is absent in the unstacked analog. A priori, such a tail could be due to either a weak optically allowed electronic state that contributes to the absorption in the stacked trimer or to broadening of the monomeric state due to coupling between the two moieties. The stacked compound shows

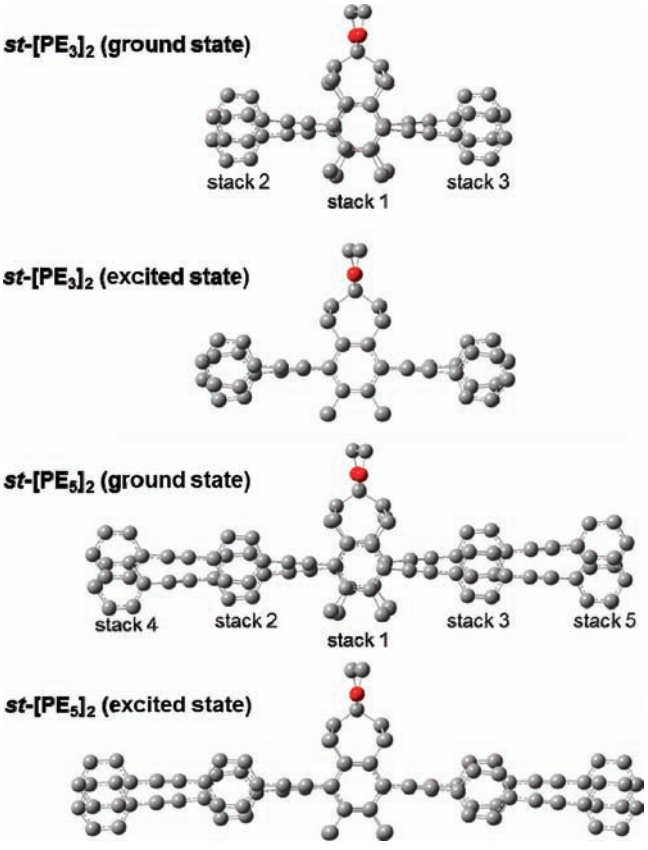

Figure 4. Sketch of the DFT-optimized geometries of the isolated ***st***-$[\mathbf{PE}_3]_2$ and ***st***-$[\mathbf{PE}_5]_2$ molecules in the ground state and in the lowest excited state; for the sake of clarity, the hydrogen atoms are not shown. The innermost pair of stacked rings is marked as stack 1; stacks 2 and 3 are next in both ***st***-$[\mathbf{PE}_3]_2$ and ***st***-$[\mathbf{PE}_5]_2$; the latter compound has additional stacks (4 and 5) at the periphery of the molecule.

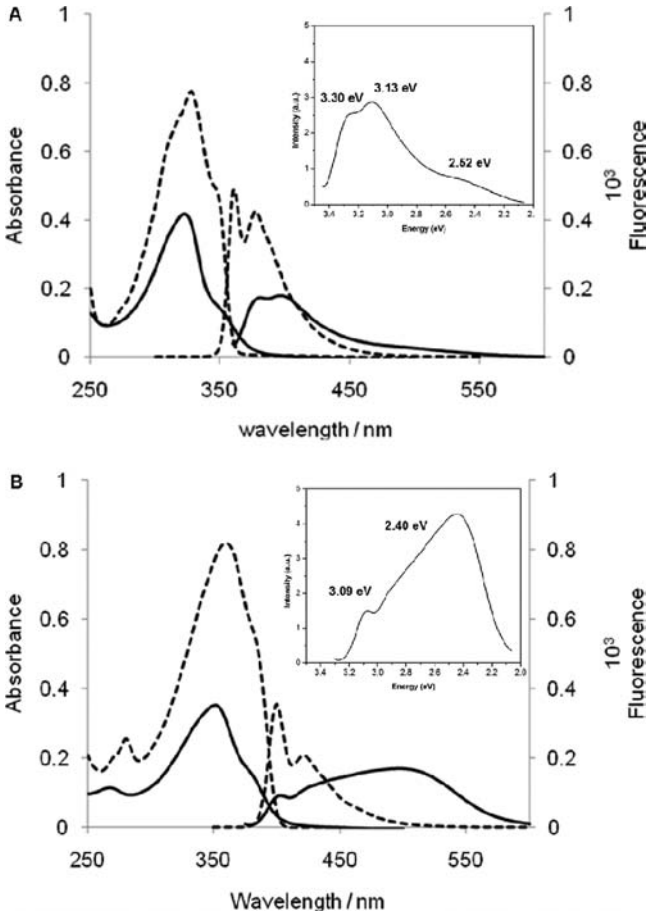

Figure 5. UV−vis and fluorescence spectra: A, ***st***-$[\mathbf{PE}_3]_2$ (solid) (c = 1.4×10^{-6} M) and $\mathbf{PE}_3$ (dotted) (c = 2.9×10^{-6} M) in $CHCl_3$, T = 23 °C; the inset depicts the emission spectra of stacked trimer on an energy scale. B, ***st***-$[\mathbf{PE}_5]_2$ (solid) (c = 0.9×10^{-6} M) and $\mathbf{PE}_5$ (dotted) (c = 1.8×10^{-6} M) in $CHCl_3$, T = 23 °C; the inset depicts the emission spectra of ***st***-$[\mathbf{PE}_5]_2$ on an energy scale.

dx.doi.org/10.1021/ja3019065 | J. Am. Chem. Soc. 2012, 134, 7176−7185

emission maxima at 382 and 397 nm, which are red-shifted from the maxima displayed by the unstacked analog (360 and 375 nm), Figure 5 and Table 2. In addition, the stacked system shows a weak emission that appears as a broad shoulder in the low-energy part of the spectrum at approximately 490 nm (~2.5 eV, see inset of Figure 5A).

Table 2. Absorption and Emission Maxima of Stacked and Unstacked PE Oligomers

	absorption (nm[35])	emission (nm[35])
[PE_3]	330	360, 375[a]
	[3.76][c]	[3.44, 3.31][c]
st-[PE_3]$_2$	325	382, 397[a], 490[b]
	[3.81][c]	[3.30, 3.13, 2.52][c]
[PE_5]	365	399, 418[a]
	[3.40][c]	[3.11, 2.97][c]
st-[PE_5]$_2$	355	398 (weak), 495 (br)
	[3.49][c]	[3.09, 2.40][c]

[a]Vibronic band. [b]Shoulder. [c]Energies for transitions are computed from deconvoluted spectra.

More pronounced differences are observed between the spectra of the pentameric homologues, *st*-[PE_5]$_2$ and PE_5. The absorption and emission maxima of both stacked and unstacked pentamers are red-shifted from those of the corresponding trimers, as expected from the greater extent of conjugation. The absorption maximum of the stacked system is again slightly blue-shifted (~90 meV) relative to the unstacked oligomer (355 nm versus 365 nm, Table 2). As in the case of stacked trimer, there is a tail at the low-energy edge in the absorption spectrum of *st*-[PE_5]$_2$. The most interesting feature, however, is that the emission spectrum of the stacked pentamer, Figure 5B, is significantly different from that of the stacked trimer. The spectrum of the stacked pentamer is dominated by a broad transition at low-energy with a maximum at ca. 495 nm. A low-intensity high-energy band is observed at 398 nm (~3.1 eV). This matches the emission maximum of the unstacked linear analog PE_5.

Analysis of the emission spectra points to the fact that at least two electronic states appear to contribute to the fluorescence of both stacked systems. In order to obtain a firm assessment of the nature of these excited states, we turn next to a discussion of the results of TD-DFT calculations of the excited states of the unstacked and stacked systems.

TD-DFT Characterization of the Excited-State Properties. To gain further insight into the effect of π-stacking on the photophysical properties of conjugated oligomers, we have optimized the geometries of the lowest excited states of the stacked systems and the unstacked model oligomers by means of TD-DFT calculations. The calculated excited-state energies are listed in Table 3. The TD-DFT $S_0 \rightarrow S_1$ transition energies of the unstacked oligomers are somewhat overestimated (~0.2 eV) compared to the experimental absorption maxima. In agreement with experiment, a ~0.3−0.4 eV decrease in S_1 energy is calculated for PE_5 compared to PE_3. In both unstacked oligomers, the S_1 state can be described essentially by a single one-electron excitation from the highest occupied molecular orbital (HOMO) to the lowest unoccupied molecular orbital (LUMO). The implicit inclusion of the solvent (geometry optimizations followed by the excited-state calculations using TD-DFT) predicts a ca. 0.1 eV decrease in optical gaps, but the trends remain the same as for the calculations on isolated molecules (see the Supporting Information). The relaxation energy (λ) of the S_1 state of PE_5 is estimated to be substantially smaller than that of PE_3 (0.06 vs 0.15 eV), which is consistent with a more delocalized nature of the excited state in the more extended system. This result is in good agreement with the observed emission spectra: with the increase in oligomer length from the trimer to the pentamer, there occurs a decrease in the ratio of the 0−1 and 0−0 vibronic peaks that are well-resolved in the emission spectra of both oligomers (Figure 5).

Table 3. DFT Estimates of the Energies in the Ground- and Excited-State Geometries, Oscillator Strength (o.s.), and Relaxation Energy λ

		energy		
molecule	state	ground state (eV) [o.s.]	excited state (eV)	λ (eV)
PE_3	S_1	4.02 [1.72]	3.53	0.15
st-[PE_3]$_2$	S_1(E)	3.70 [0.01]	2.61	0.56
	S_2(L)	4.06 [2.61]		
PE_5	S_1	3.61 [3.76]	3.21	0.06
st-[PE_5]$_2$	S_1(E)	3.41 [0.01]	2.52	0.42
	S_2(L)	3.66 [6.71]		

The TD-DFT calculations reveal that the first-excited state of both *st*-[PE_3]$_2$ and *st*-[PE_5]$_2$ is dominated by HOMO → LUMO and HOMO-1 → LUMO+1 excitations, i.e., $\psi(S_1) = a|H \rightarrow L\rangle + b|H-1 \rightarrow L+1\rangle$. Furthermore, by performing a transformation to the oligomer MO basis set (see the Supporting Information for details), $\psi(S_1)$ can be shown to correspond to a linear combination of two oligomer-localized $|AB^*\rangle$ and $|A^*B\rangle$ excitations and two interoligomer charge-transfer (CT) $|A^+B^-\rangle$ and $|A^-B^+\rangle$ excitations:[36]

$$\begin{aligned}\psi(S_1) &= a|H \rightarrow L\rangle + b|H-1 \rightarrow L+1\rangle \\ &= \left(\frac{a+b}{2}\right)(|A^*B\rangle - |AB^*\rangle) + \left(\frac{a-b}{2}\right) \\ &\quad (|A^-B^+\rangle - |A^+B^-\rangle)\end{aligned} \tag{1}$$

TD-DFT calculations carried out on the ground-state geometry indicate that the S_1 state of both systems possesses a significant CT character, ca. 15% and 10% for *st*-[PE_3]$_2$ and *st*-[PE_5]$_2$, respectively. Importantly, the CT contribution increases as the stacked systems relax to the equilibrium geometry of the S_1 state. In this case, we find that the intrachain and CT excitations contribute approximately equally to $\psi(S_1)$. We note that similar results are obtained at the semiempirical intermediate neglect of differential overlap (INDO) level of theory (see the Supporting Information). Based on these findings, we ascribe the S_1 states of the stacked systems to excimer-like states (E). As a result of their CT character, the S_1 states undergo large structural relaxations upon excitation. Thus, in the fully relaxed S_1 geometry of the stacked systems, the intercentroid distance (d_i) between the individual oligomer arms is reduced by ca. 0.20 Å compared to the ground-state geometry. This is accompanied by a decrease in the angle between the innermost benzene rings (θ_1) of 3−5° (Table 1). Such significant changes in geometry lead to relaxation energies as large as 0.5 eV. These results are consistent with the fact that low-energy emission bands are broad and structureless.

In addition, the TD-DFT calculations reveal that the S_2 states in both *st*-[PE_3]$_2$ and *st*-[PE_5]$_2$ can be described as a linear combination of the S_1 states of the individual arms. The S_2 states are thus excitonic in nature and can be assigned as local

dx.doi.org/10.1021/ja3019065 | J. Am. Chem. Soc. 2012, 134, 7176−7185

(L) states (a detailed description of the S_2 state is provided in the Supporting Information). The similarity between the energies of the S_2 states in the stacked systems and the energies of the S_1 states in the unstacked oligomers suggests that upon stacking the states of a single conjugated system are only weakly affected by interchain interactions.

The calculations also show that the difference between the energies of the excimer-like state of *st*-$[PE_3]_2$ and *st*-$[PE_5]_2$ in their relaxed geometries is very small, ca. 0.09 eV. These theoretical results agree well with the fact that the low-energy emission peaks of *st*-$[PE_3]_2$ and *st*-$[PE_5]_2$ appear at nearly the same energy (~2.4 eV, 490 nm). Inspection of the frontier orbitals contributing to the excimer-like states indicates that in the case of the stacked trimer, *st*-$[PE_3]_2$, the molecular orbitals are delocalized over the entire length of the oligomer segment. In contrast, for the stacked pentamer *st*-$[PE_5]_2$, the frontier molecular orbitals are restricted to the central three-ring section of the pentamer segments (Figure 6). This explains the similarity between the E states of *st*-$[PE_3]_2$ and *st*-$[PE_5]_2$.

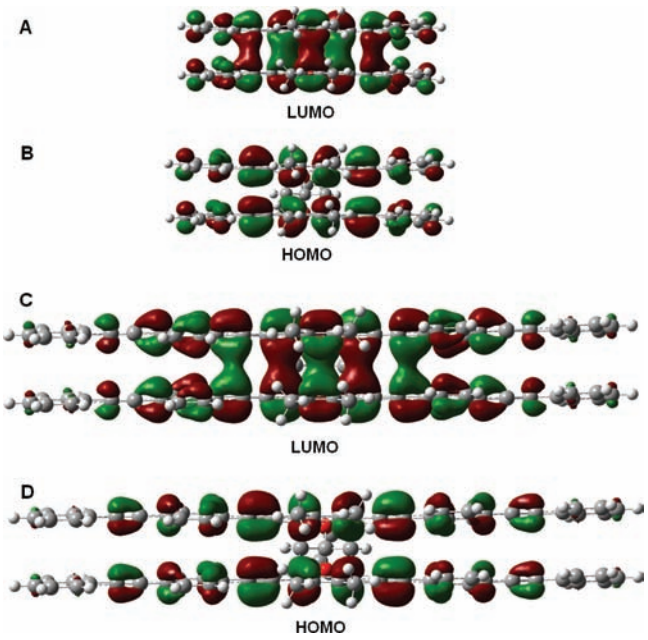

Figure 6. Frontier molecular orbitals of *st*-$[PE_3]_2$ (A and B) and *st*-$[PE_5]_2$ (C and D) of the S_1 state (in optimized geometries).

To summarize at this stage, the electronic-structure calculations indicate that (i) the absorption band and high-energy emission band in both *st*-$[PE_3]_2$ and *st*-$[PE_5]_2$ are related to the second excited state, which corresponds to the lowest excited state (L-state) of the unstacked oligomers, and (ii) the low-energy broad emission band arises from the lowest excited state, which is an excimer-like state; as a result of the large geometry relaxation, this band is significantly red-shifted in comparison to the lowest energy emission in the unstacked oligomers.

The next point is to rationalize the differences in the overall shapes of the emission spectra of *st*-$[PE_3]_2$ and *st*-$[PE_5]_2$. In general, the emission features are expected to depend on the relative populations and emission characteristics of the L and E states. Here, in the absence of temperature- and time-resolved measurements, we use a simple three-state model that is outlined in Figure 7. In this framework, the emission intensities

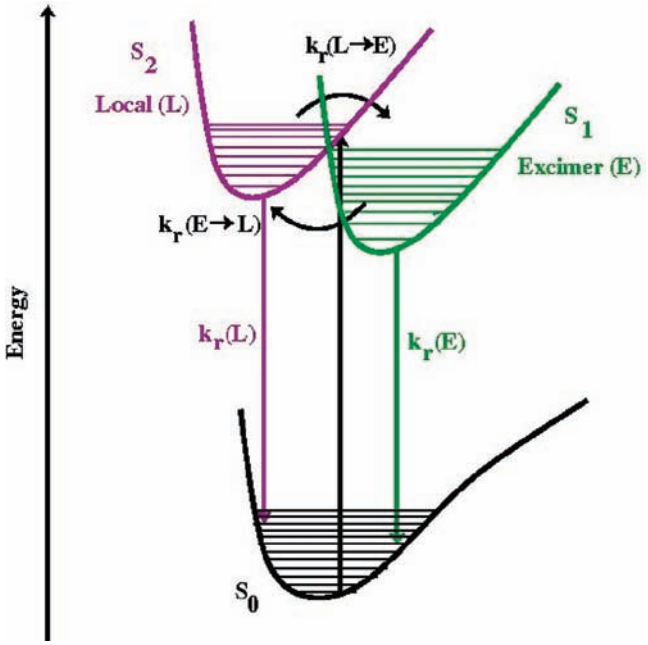

Figure 7. Schematic energy diagram showing the lowest local-excited state (L), excimer-like state (E), and ground state (S_0). The absorption, emissions from the L (k_r(L)) and E states (k_r(E)), and the forward (k_r(L → E)) and backward (k_r(E → L)) exchange between the L and the E states are also depicted.

from the relevant excited states can be analyzed following Zachariasse and co-workers by using the rate equation described by eq 2.[37] The ratio of emission intensities from the E and L states (i.e., I(E)/I(L)) can then be written as

$$\frac{I(\mathrm{E})}{I(\mathrm{L})} = \frac{k_r(\mathrm{E})}{k_r(\mathrm{L})}\frac{k_r(\mathrm{L}\rightarrow\mathrm{E})\tau_0(\mathrm{E})}{k_r(\mathrm{E}\rightarrow\mathrm{L})\tau_0(\mathrm{E}) + 1} \qquad (2)$$

where k_r(E) and k_r(L) are the radiative rate constants of the E and L states, k_r(L→E) and k_r(E→L) are the forward and backward reaction rates between the local and excimer-like states, and τ_0(E) is the fluorescence lifetime of the E state. While a detailed investigation of these kinetic processes is beyond the scope of this work, the main differences between the emission patterns in *st*-$[PE_3]_2$ and *st*-$[PE_5]_2$ can be analyzed on the basis of the spectroscopic and theoretical data presented above. The TD-DFT calculations indicate that k_r(E)/k_r(L) is of the order of 10^{-2} for both stacked systems. This suggests that the difference between the emission intensities of *st*-$[PE_3]_2$ and *st*-$[PE_5]_2$ is related to the second factor in eq 2

$$\frac{k_r(\mathrm{L}\rightarrow\mathrm{E})\tau_0(\mathrm{E})}{k_r(\mathrm{E}\rightarrow\mathrm{L})\tau_0(\mathrm{E}) + 1} = B(\mathrm{L}\rightarrow\mathrm{E}) \qquad (3)$$

when k_r(E→L)τ_0(E) ≫ 1, one obtains B(L → E) = k_r(L → E)/k_r(E → L) and parameter B is then proportional to the free energy difference (driving force), ΔG^0, related to the L → E transition. This approximation turns out to work well for *st*-$[PE_5]_2$. Indeed, using the experimental energies and the calculated relaxation energies, we estimate for this system that $\Delta G^0 \approx 0.40$ eV and k_r(L → E)/k_r(E → L) ≈ 10^4. The ratio of the forward and backward rates, along with the value of 10^{-2} derived for k_r(E)/k_r(L), is consistent with the much stronger emission from the excimer-like state than from the local state by approximately 2 orders of magnitude. The lower bound for k_r(L → E) in this case is given by the condition k_r(L → E)τ_0(E)

dx.doi.org/10.1021/ja3019065 | J. Am. Chem. Soc. 2012, 134, 7176–7185

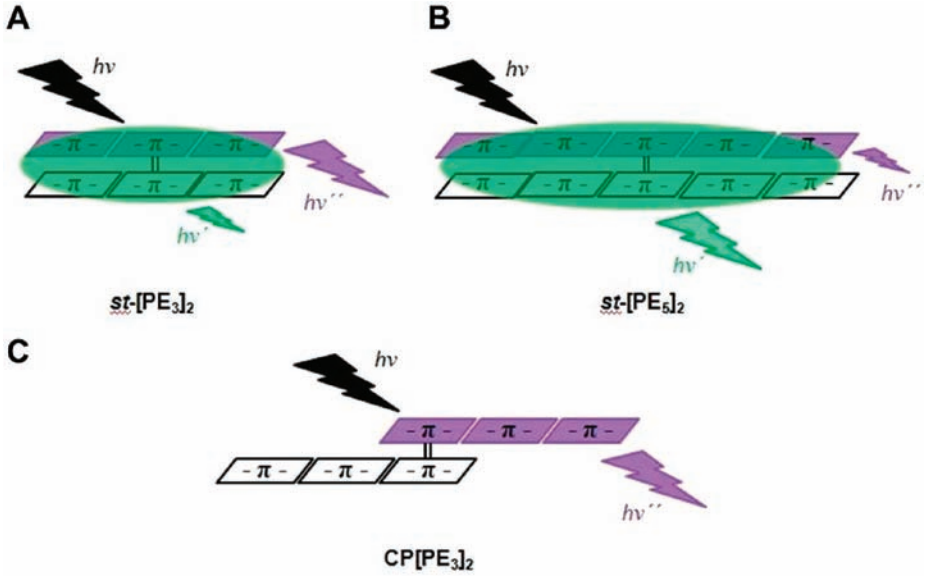

Figure 8. Schematic representation of the photophysical behavior of benzo-fused bicyclo[4.4.1]undecane stacked oligo(phenylene ethynylene)s, ***st***-$[\mathbf{PE}_3]_2$ (A) and ***st***-$[\mathbf{PE}_5]_2$ (B), and pseudopara [2.2]paracyclophane based stacked compound, $\mathbf{CP}[\mathbf{PE}_3]_2$ (**C**).

> 10^4. We note that in related cofacially stacked perylene-diimide dimers, τ_0 was found to be about 10^{-7} s.[38] Assuming a similar value for τ_0 in the present systems leads to $k_r(L \rightarrow E) > 10^{11}$ s^{-1} for ***st***-$[\mathbf{PE}_5]_2$. In the case of ***st***-$[\mathbf{PE}_3]_2$, we estimate $\Delta G^0 \approx 0.24$ eV and $k_r(L \rightarrow E)/k_r(E \rightarrow L) \approx 10^7$. These results suggest that for ***st***-$[\mathbf{PE}_3]_2$ the product $k_r(E \rightarrow L)\tau_0(E)$ is less than one and that the parameter B is $k_r(L \rightarrow E)\tau_0(E)$. According to eq 1 and recalling that $k_r(E)/k_r(L) \approx 10^{-2}$, the product $k_r(L \rightarrow E)\tau_0(E)$ should then be smaller than 100 in order to reproduce a stronger emission from the local state than from the excimer-like state, as is experimentally observed. This result sets an upper bound for the forward reaction rate in ***st***-$[\mathbf{PE}_3]_2$ with $k_r(L \rightarrow E) < 10^9$ s^{-1}. Based on the constraints that this analysis places on the forward rate constant $k_r(L \rightarrow E)$, the activation barrier for the transition from the local excited state to the excimer-like state in ***st***-$[\mathbf{PE}_3]_2$ is at least 0.1 eV larger than in ***st***-$[\mathbf{PE}_5]_2$.

Thus, this simple three-level model provides a reasonable description of the difference in the emission spectra of ***st***-$[\mathbf{PE}_3]_2$ and ***st***-$[\mathbf{PE}_5]_2$ by correlating the relative populations in the local (L) and excimer-like (E) states. For both stacked molecules, absorption leads to population of the L-state. This is followed by a substantial geometric relaxation. By comparing the experimental absorption and emission spectra of the stacked and unstacked molecules, such a relaxation is found to be on the order of 0.4 eV. The TD-DFT results are in good agreement with the experimental observations. For ***st***-$[\mathbf{PE}_3]_2$, the emission spectra is dominated by a radiative transition from the L-state, as depicted in Figure 8A. In addition to this process, a small fraction of the locally excited population decays into the low-lying excimer-like state. However, a relatively high activation barrier restricts the excited-state population such that emission from the higher-energy L-state predominates. Thus, the presence of the low-lying E-state results only in a broad tail in the emission spectra, which is absent in the corresponding unstacked analogue, $\mathbf{PE}_3$. In contrast, for ***st***-$[\mathbf{PE}_5]_2$ the activation barrier appears to be lower than for ***st***-$[\mathbf{PE}_3]_2$. As a consequence, there is a significant transfer of population from the L-state to the E-state, leading to a significant red-shift in emission, see Figure 8B.

Interestingly, cyclophane-type stacked compounds, e.g., $\mathbf{CP}[\mathbf{PE}_3]_2$ in Figure 1, which provide for spatially limited interchain interactions (i.e., only between the phenyl rings within the cycolphane core), do not present contributions from excimer-like states in their photophysics. Thus, it is important to note that the design of the stacked molecules achieved in the present work significantly modifies the low-energy photophysics compared to that of the pseudopara substituted stacked cyclophane. In the latter case, the excimer-like state ("phane-state") remains higher in energy compared to the L-state, particularly for longer oligomers. As a consequence, the emission of $\mathbf{CP}[\mathbf{PE}_3]_2$ is dominated by the local L-state, with no contribution from the E-state, as shown in Figure 8C, in contrast to the emission from the longer bicycloundecanone-stacked oligo(phenylene ethynylene).

■ CONCLUSIONS

A combined experimental and theoretical study of well-defined stacked oligo(phenylene ethynylene)s provides very useful insights into the effect of $\pi-\pi$ interactions on the electronic structure of closely packed conjugated chains. Our synthetic strategy results in molecular architectures in which conjugated units are stacked atop one another in such a way that strong electronic interactions occur over the entire length of the chromophoric moieties.

The absorption and emission spectra of the stacked compounds were compared to those of the individual unstacked oligomers. These optical studies, when analyzed together with the results of TD-DFT calculations, clearly demonstrate the effect of interchain interactions on the low-energy photophysics of stacked compounds. A simple three-state model provides an explanation for the large red shift observed in ***st***-$[\mathbf{PE}_5]_2$ compared to its shorter analogue ***st***-$[\mathbf{PE}_3]_2$. The origin of the shift lies in the competition between emission from a local excited state and from an excimer-like state.

dx.doi.org/10.1021/ja3019065 | *J. Am. Chem. Soc.* 2012, 134, 7176−7185

Interestingly, cyclophane-type stacked compounds, which provide for spatially limited interchain interactions, do not present contributions from excimer-like states in their photophysics. Thus, stacked molecules such as ***st*-[PE$_3$]$_2$** and ***st*-[PE$_5$]$_2$** serve as better-suited platforms to develop an understanding of the interactions between cofacially stacked conjugated chains, since they more closely resemble the arrangement of the π-systems of semiconducting organic oligomers and polymers in thin-film organic electronic devices.

EXPERIMENTAL SECTION

General Synthetic Methods. All starting materials were purchased from commercial sources and used without further purification unless there otherwise stated. THF was dried over sodium benzophenone ketyl prior to distillation under argon. Thin-layer chromatography (TLC) and column chromatography were performed on flash grade silica (32−60 Å, Sorbent Technologies, Atlanta, GA). NMR analysis was performed on a Bruker DSX 300 instrument using $CDCl_3$ as the solvent. Chemical shifts are referenced to internal tetramethylsilane. IR analyses were performed on a Nicolet 4700 FTIR with an ATIR attachment from Smart-Orbit Thermoelectronic Corporation. Ultraviolet−visible analysis was performed on a Shimadzu UV-2401PC spectrometer, and fluorescence spectroscopy was performed on a Shimadzu RF-5301PC spectrofluorometer. Mass spectra were determined on a VG-70SE instrument.

Ketone **1** was prepared using similar synthetic procedures to those reported by Mataka[24] for the preparation of analogous compound lacking the four methyl groups (see the Supporting Information). Synthetic procedures and characterization data for the compounds **2**, **3** [PE$_3$]$_2$, ***st*-[PE$_3$]$_2$**, [PE$_5$]$_2$, and ***st*-[PE$_5$]$_2$** are described below.

Ethylene Acetal of Tetramethyl Dibenzo[3,4-c:8,9-c']-bicyclo[4.4.1]undecan-11-one, 3. A solution of **1** (100 mg, 310 μmol), ethylene glycol (200 mg, 3.23 mmol), and *p*-toluenesulfonic acid (1 mg) in benzene (50 mL) was heated at reflux for 48 h with removal of water via a Dean−Stark trap. The solvent was removed under reduced pressure and the residue was subjected to column chromatography (CH_2Cl_2) followed by recrystallization from hexanes to give the title compound (95 mg, 84%) as a yellow crystalline solid. MP = 217−218 °C. ^{1}H NMR (300 MHz, $CDCl_3$): δ 6.40 (s, 4H, Ar−H), 4.05 (s, 4H, OCH_2CH_2O), 3.34 (dd, J = 15, 2 Hz, 4H, axial benzylic), 2.58 (dd, J = 15, 6 Hz, 4H, equatorial benzylic), 2.24 (m, 2H, bridgehead), 1.98 (s, 12H, Ar−CH_3). ^{13}C NMR (75 MHz, $CDCl_3$): δ 135.4 (O−C−C-O), 133.8, 132.7, 127.3 (aromatic), 64.8 (−OCH_2−), 45.8 (bridgehead), 31.1 (benzylic), 19.2 (ArCH_3). IR (ATR): 2997, 2930, 2877, 1439, 1383, 1110, 1040, 891 cm^{-1}. MS (MALDI), m/z (%) = 362.2 (M$^+$, 70), 229.0 (100), 104.9 (75). HRMS (EI), m/z = Calcd. For $C_{25}H_{30}O_2$, 362.2246; Found, 362.2249, Δ = 0.8 ppm.

Tetraiodide, 2. Iodine (0.62 g, 5.0 mmol) was added to a solution of **1** (200 mg, 620 μmol) and mercury(II) trifluoromethanesulfonate (1.89 g, 3.72 mmol) in CH_2Cl_2 (10 mL) in an oven-dried Shlenk flask. The mixture was stirred for 16 h, and CH_2Cl_2 (50 mL) was added. The mixture was filtered and the organic layer was washed with a saturated solution of $Na_2S_2O_3$ (50 mL) followed by a saturated solution of KI (50 mL). The organic layer was dried over $MgSO_4$ and the solvent was removed under reduced pressure to give a yellow residue. ^{1}H NMR analysis showed the presence of residual hydrogen atoms on aromatic rings. Accordingly, the residue was resubjected to iodination. Following workup, the residue was triturated with boiling hexane and filtered to give the title compound as a white solid (0.4 g, 74%). MP = 216−217 °C. ^{1}H NMR (300 MHz, $CDCl_3$): δ 2.40−3.60 (br m, 10H, benzylic and bridgehead), 2.10−2.40 (br s, 12H, Ar−CH_3). Low solubility of the product precluded analysis by ^{13}C NMR spectroscopy. IR (ATR): 2914, 2854, 1711, 1493, 1163, 1007, 881, 738 cm^{-1}. MS (MALDI), m/z (%) = 821.8 (M$^+$, 100). HRMS (EI), m/z = Calcd. For $C_{23}H_{24}OI_4$, 821.7802; Found, 821.7810, Δ = 0.9 ppm.

Trimer-Fused Bicycloundecanone, [PE$_3$]$_2$. A solution of **2** (350 mg, 420 μmol), $Pd(PPh_3)_2Cl_2$ (56 mg, 80 μmol), CuI (16 mg, 80 μmol), and PPh_3 (21 mg, 80 μmol) in a 1:1 v/v mixture of DIPA and THF (5 mL) was degassed using three cycles of freeze−pump−thaw and back-purged with argon. Phenylacetylene (257 mg, 2.52 mmol) was added dropwise and the mixture was heated at reflux for 48 h. CH_2Cl_2 (50 mL) was added and the solution was washed sequentially with saturated aqueous NH_4Cl (50 mL) and H_2O (50 mL). The organic layer was dried over $MgSO_4$ and the solvent was removed under reduced pressure. The residue was dissolved in CH_2Cl_2 (5 mL) and flushed through a silica gel column with CH_2Cl_2. The solvent was removed under reduced pressure and the residue was recrystallized from THF to afford the title compound as a yellow solid (150 mg, 49%). MP = 309−310 °C. ^{1}H NMR (300 Hz, $CDCl_3$): δ 7.20−7.80 (m, 20H, Ar−H), 2.82−4.30 (br m, 10H, benzylic and bridgehead), 2.40−2.70 (br s, 12H, Ar−CH_3). The low solubility of the product precluded analysis by ^{13}C NMR spectroscopy. IR (ATR): 2997, 2954, 2877, 1736, 1465, 1110, 943 cm^{-1}. MS (MALDI), m/z (%) = 718.4 (M+, 80). HRMS (EI), m/z = Calcd. For $C_{55}H_{42}O$, 718.3235; Found, 718.3192, Δ = 5.9 ppm.

Stacked Trimer, *st*-[PE$_3$]$_2$. [PE$_3$]$_2$ (100 mg, 140 μmol) was subjected to ketalization with ethylene glycol (200 mg, 3.23 mmol) in the presence of *p*-toluenesufonic acid (1 mg) in benzene (50 mL) according to the procedure described above for the synthesis of **3**. The product obtained from column chromatography was triturated with hexanes to give the title compound as a yellow solid (90 mg, 85%). MP = 295−296 °C. ^{1}H NMR (300 MHz, CD_2Cl_2): δ 7.28−7.38 (m, 8H, Ar−H), 7.08−7.24 (m, 12H, Ar−H), 4.10 (s, 4H, −OCH_2CH_2O−) 3.79 (dd, 4H, J = 16, 6 Hz, equatorial benzylic), 3.30 (dd, 4H, J = 15, 2 Hz, axial benzylic), 2.45−2.58 (m, 2H, bridgehead), 2.38 (s, 12 H, Ar−CH_3). ^{13}C NMR (75 MHz, $CDCl_3$): δ 218.1 (C═O), 154.2, 152.1, 139.3, 138.6, 134.2, 133.2, 131.5 (aromatic), 71.1, 70.5 (−OCH_2−), 52.2 (bridgehead), 39.4, 35.0 (benzylic), 19.2 (methyl). IR (ATR): 2988, 2938, 2877, 1608, 1502, 1105, 1077, 987 cm^{-1}. MS (MALDI), m/z (%) = 762.3 (M$^+$, 80). HRMS (EI), m/z = Calcd. For $C_{57}H_{46}O_2$, 762.3497; Found, 762.3339, Δ = 20.8 ppm.

Pentamer-Fused Bicycloundecanone, [PE$_5$]$_2$. (4-(Phenylethynyl)phenyl)acetylene (430 mg, 2.20 mmol) was added to a solution of **2** (300 mg, 0.36 mmol), $Pd(PPh_3)_2Cl_2$ (56 mg, 80 μmol), CuI (16 mg, 80 μmol) and PPh_3 (21 mg, 80 μmol) in a 1:1 v/v mixture of DIPA/THF (10 mL) according the procedure described above for the preparation of [PE$_3$]$_2$. The reaction mixture was cooled to room temperature and poured into MeOH (200 mL). The precipitated solid was removed by filtration and recrystallized from THF to afford the title product as a green solid (120 mg, 30%). MP = 380 °C (decomposes). ^{1}H NMR (300 Hz, $C_2D_2Cl_4$, 80 °C): δ 7.20−7.70 (m, 36H, Ar−H), 2.82−4.20 (br m, 10H, benzylic and bridgehead), 2.40−2.70 (br s, 12 H, Ar−CH_3). The low solubility of the product precluded analysis by ^{13}C NMR spectroscopy. IR (ATR): 2992, 2958, 2862, 1720, 1475, 1103, 932 cm^{-1}. MS (MALDI), m/z (%) = 1118.4 (M$^+$, 80). HRMS (EI), m/z = Calcd. For $C_{87}H_{58}O$, 1118.449; Found, 1118.439, Δ = 9.0 ppm.

Stacked pentamer, *st*-[PE$_5$]$_2$. [PE$_5$]$_2$ (100 mg, 90 μmol) was subjected to ketalization with ethylene glycol (200 mg, 3.23 mmol) in the presence of *p*-toluenesulfonic acid (1 mg) in benzene (50 mL) according to the procedure provided above for the preparation of ***st*-[PE$_3$]$_2$** to give the title compound as a green solid (85 mg, 82%). MP = 354 °C (decomposes). ^{1}H NMR (300 MHz, $CDCl_3$): δ 7.40−7.47 (m, 8H, Ar−H), 7.16−7.34 (m, 28H, Ar−H), 4.18 (s, 4H, −OCH_2CH_2O−) 3.84 (dd, 4H, J = 15, 6 Hz, equatorial benzylic), 3.30 (dd, 4H, J = 15, 2 Hz, axial benzylic), 2.45−2.58 (m, 2 H, bridgehead), 2.38 (s, 12 H, Ar−CH_3). The low solubility of the product precluded analysis by ^{13}C NMR spectroscopy. IR (ATR): 2987, 2934, 2867, 1615, 1510, 1109, 1065, 988 cm^{-1}. MS (MALDI), m/z (%) = 1162.4 (M$^+$, 80). HRMS (EI), m/z = Calcd. For $C_{89}H_{62}O_2$, 1162.47498; Found, 1162.4546, Δ = 17.5 ppm.

Linear Unstacked Trimer, PE$_3$. A solution of 2,3,5,6-tetramethyl-1,4-diiodobenzene (500 mg, 1.30 mmol), $Pd(Ph_3P)Cl_2$ (50 mg, 70 μmol), CuI (15 mg, 70 μmol) and phenylacetylene (450 mg, 4.00 mmol) in a 1:1 v/v mixture of THF and piperidine (10 mL) was stirred for 36 h under Ar. CH_2Cl_2 (50 mL) was added and the solution

dx.doi.org/10.1021/ja3019065 | J. Am. Chem. Soc. 2012, 134, 7176−7185

was washed with sat. NH_4Cl (100 mL) and H_2O (100 mL). The solvent was removed under reduced pressure and the residue was subjected to column chromatography (CH_2Cl_2) followed by recrystallization from hexane to afford the title compound as a yellow solid (400 mg, 93% yield). MP = 218−219 °C. ^{1}H NMR ($CDCl_3$): δ 7.53−7.59 (m, 4H, Ar−H), 7.33−7.38 (m, 6H, Ar−H), 2.50 (s, 12H, Ar−CH_3). ^{13}C NMR ($CDCl_3$): δ 135.7, 131.4, 128.4, 128.1, 123.9, 123.3 (aromatic), 98.1, 88.6 (−C≡C−), 18.4 (Ar−CH_3). IR (ATR): 3066, 3036, 2927, 1598, 1495, 1017, 752 cm^{-1}. MS (EI): m/z (%) 334.1 (M^+, 100), 167.1 (20). HRMS (EI), m/z = Calcd. For $C_{26}H_{22}$, 334.1722; Found 334.1753, Δ = 9.3 ppm.

Linear Unstacked Pentamer PE_5. A solution of 2,3,5,6-tetramethyl-1,4-diiodobenzene (250 mg, 650 μmol), $Pd(Ph_3P)Cl_2$ (23 mg, 30 μmol), CuI (6.0 mg, 30 μmol) and (4-(phenylethynyl)-phenyl)acetylene (404 mg, 2.00 mmol) was treated according to the procedure provided above for the preparation of PE_3. . The product obtained from column chromatography was triturated with hexanes to afford the title compound as a yellow solid (330 mg, 96% yield). MP = 254−255 °C. ^{1}H NMR ($CDCl_3$): δ 7.50−7.59 (m, 12H, Ar−H), 7.31−7.40 (m, 6H, Ar−H), 2.51 (s, 12H, Ar−CH_3). The low solubility of the product precluded analysis by ^{13}C NMR spectroscopy. IR (ATR, neat): 3072, 3024, 2936, 1585, 1487, 1024, 751 cm^{-1}. MS (EI): m/z (%) 534.2 (M^+, 100), 267.2 (10). HRMS (EI), m/z = Calcd. For $C_{42}H_{30}$, 534.2348; Found 534.2340, Δ = 1.5 ppm.

Computational Studies. The geometry optimizations of the unstacked molecules (PE_3 and PE_5) were performed using both B3LYP and ωB97X/6-31g* functionals[39] and the 6-31g* basis set. To account for the dispersion interactions between the oligomer moieties of the stacked molecules *st*-$[PE_3]_2$ and *st*-$[PE_5]_2$, the geometries were obtained at the ωB97X-D/6-31g*[40] level of theory. The geometry optimizations were performed for the isolated molecules and by using the continuum solvent model to implicitly account for the effect of $CHCl_3$ solvent. All geometries were confirmed to be minima by additional vibrational frequency calculations. The low-lying excited states were derived using time-dependent density functional theory (TD-DFT) using the 6-31g* basis set and the long-range corrected functionals ωB97X-D and ωB97X for the stacked and unstacked molecules, respectively. Recent investigations have indicated that long-range corrected functionals largely mitigate the issue related to the spurious electron self-interaction characteristic of standard generalized gradient functionals and provide a reliable description of charge-transfer excitations.[39−42] We note that high-level wave function methods based on multireference perturbation theory[36] have recently been successfully applied to investigate the excimer states of various oligoacene dimers. However, these approaches quickly become prohibitively and time-consuming when geometry optimizations of the excited states are required, as is the case for the present investigations. Accordingly, we conducted TD-DFT calculations at the same level of theory as that used for the ground-state calculations to obtain the optimal geometries of the lowest excited states of the stacked and unstacked systems. All DFT calculations were performed using the Gaussian 09 package.[43]

■ ASSOCIATED CONTENT

Ⓢ Supporting Information

Synthetic procedures and structural characterization of stacked compounds and unstacked linear models; TD-DFT results when considering a dielectric medium corresponding to $CHCl_3$; and coordinates of the DFT-optimized isolated stacked (*st*-$[PE_3]_2$ and *st*-$[PE_5]_2$) and unstacked (PE_3 and PE_5) oligomers in the ground and excited states. This material is available free of charge via the Internet at http://pubs.acs.org.

■ AUTHOR INFORMATION

Corresponding Author

david.collard@chemistry.gatech.edu

Notes

The authors declare no competing financial interest.

■ ACKNOWLEDGMENTS

The research program on stacked conjugated oligomers in the Collard group was initiated with the support of the National Science Foundation (Award ECCS-437925). We thank the Georgia Tech Center for Organic Photonics and Electronics (COPE) for scholarship support provided to S.P.J. The work in the Brédas group is supported by the STC program of the National Science Foundation under Award DMR-0120967.

■ REFERENCES

(1) Bredas, J. L.; Beljonne, D.; Coropceanu, V.; Cornil, J. *Chem. Rev.* **2004**, *104*, 4971.
(2) Bredas, J. L.; Cornil, J.; Beljonne, D.; dos Santos, D.; Shuai, Z. G. *Acc. Chem. Res.* **1999**, *32*, 267.
(3) Cornil, J.; dos Santos, D. A.; Crispin, X.; Silbey, R.; Bredas, J. L. *J. Am. Chem. Soc.* **1998**, *120*, 1289.
(4) Bredas, J. L.; Street, G. B. *Acc. Chem. Res.* **1985**, *18*, 309.
(5) Warshel, A.; Karplus, M. *J. Am. Chem. Soc.* **1972**, *94*, 5612.
(6) Yang, S. C.; Graupner, W.; Guha, S.; Puschnig, P.; Martin, C.; Chandrasekhar, H. R.; Chandrasekhar, M.; Leising, G.; Ambrosch-Draxl, C.; Scherf, U. *Phys. Rev. Lett.* **2000**, *85*, 2388.
(7) Moliton, A.; Hiorns, R. C. *Polym. Int.* **2004**, *53*, 1397.
(8) Jenekhe, S. A.; Osaheni, J. A. *Science* **1994**, *265*, 765.
(9) Sluch, M. I.; Godt, A.; Bunz, U. H. F.; Berg, M. A. *J. Am. Chem. Soc.* **2001**, *123*, 6447.
(10) Garnier, F.; Hajlaoui, R.; Yassar, A.; Srivastava, P. *Science* **1994**, *265*, 1684.
(11) Sirringhaus, H.; Tessler, N.; Friend, R. H. *Science* **1998**, *280*, 1741.
(12) Katz, H. E.; Lovinger, A. J.; Johnson, J.; Kloc, C.; Siegrist, T.; Li, W.; Lin, Y. Y.; Dodabalapur, A. *Nature* **2000**, *404*, 478.
(13) Burroughes, J. H.; Bradley, D. D. C.; Brown, A. R.; Marks, R. N.; Mackay, K.; Friend, R. H.; Burns, P. L.; Holmes, A. B. *Nature* **1990**, *347*, 539.
(14) Sheats, J. R.; Antoniadis, H.; Hueschen, M.; Leonard, W.; Miller, J.; Moon, R.; Roitman, D.; Stocking, A. *Science* **1996**, *273*, 884.
(15) Friend, R. H.; Gymer, R. W.; Holmes, A. B.; Burroughes, J. H.; Marks, R. N.; Taliani, C.; Bradley, D. D. C.; Dos Santos, D. A.; Bredas, J. L.; Logdlund, M.; Salaneck, W. R. *Nature* **1999**, *397*, 121.
(16) Sariciftci, N. S.; Smilowitz, L.; Heeger, A. J.; Wudl, F. *Science* **1992**, *258*, 1474.
(17) Halls, J. J. M.; Walsh, C. A.; Greenham, N. C.; Marseglia, E. A.; Friend, R. H.; Moratti, S. C.; Holmes, A. B. *Nature* **1995**, *376*, 498.
(18) Yu, G.; Gao, J.; Hummelen, J. C.; Wudl, F.; Heeger, A. J. *Science* **1995**, *270*, 1789.
(19) Bartholomew, G. P.; Bazan, G. C. *Acc. Chem. Res.* **2001**, *34*, 30.
(20) Morisaki, Y.; Chujo, Y. *Prog. Polym. Sci.* **2008**, *33*, 346.
(21) Salhi, F.; Lee, B.; Metz, C.; Bottomley, L. A.; Collard, D. M. *Org. Lett.* **2002**, *4*, 3195.
(22) Guyard, L.; Audebert, P. *Electrochem. Commun.* **2001**, *3*, 164.
(23) Song, C.; Swager, T. M. *Org. Lett.* **2008**, *10*, 3575.
(24) Mataka, S.; Takahashi, K.; Mimura, T.; Hirota, T.; Takuma, K.; Kobayashi, H.; Tashiro, M.; Imada, K.; Kuniyoshi, M. *J. Org. Chem.* **1987**, *52*, 2653.
(25) Mataka, S.; Shigaki, K.; Sawada, T.; Mitoma, Y.; Taniguchi, M.; Thiemann, T.; Ohga, K.; Egashira, N. *Angew. Chem., Int. Ed.* **1998**, *37*, 2532.
(26) Knoblock, K. M.; Silvestri, C. J.; Collard, D. M. *J. Am. Chem. Soc.* **2006**, *128*, 13680.
(27) Chebny, V. J.; Shukla, R.; Lindeman, S. V.; Rathore, R. *Org. Lett.* **2009**, *11*, 1939.
(28) Morisaki, Y.; Sawamura, T.; Murakami, T.; Chujo, Y. *Org. Lett.* **2010**, *12*, 3188.
(29) Giaimo, J. M.; Lockard, J. V.; Sinks, L. E.; Scott, A. M.; Wilson, T. M.; Wasielewski, M. R. *J. Phys. Chem. A* **2008**, *112*, 2322.
(30) Mangalum, A.; Morgan, B. P.; Hanley, J. M.; Jecen, K. M.; McGill, C. J.; Robertson, G. A.; Smith, R. C. *Chem. Commun.* **2010**, *46*, 5136.

(31) Kaikawa, T.; Takimiya, K.; Aso, Y.; Otsubo, T. *Org. Lett.* **2000**, *2*, 4197.
(32) Bazan, G. C.; Oldham, W. J.; Lachicotte, R. J.; Tretiak, S.; Chernyak, V.; Mukamel, S. *J. Am. Chem. Soc.* **1998**, *120*, 9188.
(33) Cornil, J.; Beljonne, D.; Calbert, J. P.; Bredas, J. L. *Adv. Mater.* **2001**, *13*, 1053.
(34) Karplus, M. *J. Am. Chem. Soc.* **1963**, *85*, 2870.
(35) Veldman, D.; Chopin, S. M. A.; Meskers, S. C. J.; Groeneveld, M. M.; Williams, R. M.; Janssen, R. A. J. *J. Phys. Chem. A* **2008**, *112*, 5846.
(36) Shirai, S.; Iwata, S.; Tani, T.; Inagaki, S. *J. Phys. Chem. A* **2011**, *115*, 7687.
(37) Druzhinin, S. I.; Ernsting, N. P.; Kovalenko, S. A.; Lustres, L. W.; Senyushkina, T. A.; Zachariasse, K. A. *J. Phys. Chem. A* **2006**, *110*, 2955.
(38) Veldman, D.; Chopin, S. M. A.; Meskers, S. C. J.; Janssen, R. A. J. *J. Phys. Chem. A* **2008**, *112*, 8617.
(39) Chai, J. D.; Head-Gordon, M. *J. Chem. Phys.* **2008**, *128*, 084106.
(40) Chai, J. D.; Head-Gordon, M. *Phys. Chem. Chem. Phys.* **2008**, *10*, 6615.
(41) Stein, T.; Kronik, L.; Baer, R. *J. Chem. Phys.* **2009**, *131*, 244119.
(42) Stein, T.; Kronik, L.; Baer, R. *J. Am. Chem. Soc.* **2009**, *131*, 2818.
(43) Frisch, M. J. T., G. W.; Schlegel, H. B.; Scuseria, G. E.; Robb, M. A.; Cheeseman, J. R.; Montgomery, Jr., J. A.; Vreven, T.; Kudin, K. N.; Burant, J. C.; Millam, J. M.; Iyengar, S. S.; Tomasi, J.; Barone, V.; Mennucci, B.; Cossi, M.; Scalmani, G.; Rega, N.; Petersson, G. A.; Nakatsuji, H.; Hada, M.; Ehara, M.; Toyota, K.; Fukuda, R.; Hasegawa, J.; Ishida, M.; Nakajima, T.; Honda, Y.; Kitao, O.; Nakai, H.; Klene, M.; Li, X.; Knox, J. E.; Hratchian, H. P.; Cross, J. B.; Bakken, V.; Adamo, C.; Jaramillo, J.; Gomperts, R.; Stratmann, R. E.; Yazyev, O.; Austin, A. J.; Cammi, R.; Pomelli, C.; Ochterski, J. W.; Ayala, P. Y.; Morokuma, K.; Voth, G. A.; Salvador, P.; Dannenberg, J. J.; Zakrzewski, V. G.; Dapprich, S.; Daniels, A. D.; Strain, M. C.; Farkas, O.; Malick, D. K.; Rabuck, A. D.; Raghavachari, K.; Foresman, J. B.; Ortiz, J. V.; Cui, Q.; Baboul, A. G.; Clifford, S.; Cioslowski, J.; Stefanov, B. B.; Liu, G.; Liashenko, A.; Piskorz, P.; Komaromi, I.; Martin, R. L.; Fox, D. J.; Keith, T.; Al-Laham, M. A.; Peng, C. Y.; Nanayakkara, A.; Challacombe, M.; Gill, P. M. W.; Johnson, B.; Chen, W.; Wong, M. W.; Gonzalez, C.; Pople, J. A *Gaussian 09*, revision A.02; Gaussian Inc.: Wallingford CT, 2009.